Existence of steady-state black hole analogs in finite quasi-one-dimensional Bose-Einstein condensates

Caio C. Holanda Ribeiro, Sang-Shin Baak, and Uwe R. Fischer
Seoul National University, Department of Physics and Astronomy, Center for Theoretical Physics, Seoul 08826, Korea

(Received 22 January 2022; accepted 2 June 2022; published 27 June 2022)

We theoretically propose a finite-size quasi-one-dimensional Bose-Einstein condensate with coherent source and drain placed at its two ends, which can in principle sustain a stationary sonic black hole with a single event horizon. Our analysis is focused on the condensate persistence against quantum fluctuations. We show that similar to black hole-white hole pairs, dynamical instabilities occur. Investigating in detail the instabilities' dependence on the system parameters, we also identify windows of formally infinite black hole lifetimes. By using quantum depletion of the condensate as a diagnostic tool, we validate the usage of Bogoliubov theory to describe the analog Hawking process, and establish novel signatures of Hawking radiation in the depleted cloud, both inside and outside the event horizon.

DOI: 10.1103/PhysRevD.105.124066

I. INTRODUCTION

The discovery by Stephen Hawking that black holes, quantum mechanically, are not black but radiate a thermal spectrum of particles [1,2] continues to furnish an intriguing milestone in the quest for a unification of quantum mechanics with gravity [3]. While an observation of the Hawking effect with astrophysical black holes is essentially impossible, analog systems in fluids have enabled it due to its kinematical nature [4–7] and robustness against (most variants of) Lorentz invariance breaking [8–11]. In particular, Bose-Einstein condensates have been identified as suitable system to verify an analog of Hawking's prediction in a superfluid of very low temperature, and other quantum effects related to sonic horizons see, e.g., [12–24].

An unambiguous confirmation of the quantum Hawking effect was achieved in 2019 by the Steinhauer group [25], see also the more recent experiment [26]. The observation of the density-density correlations as a second-order correlation function signature of the Hawking effect [18,27,28], however, still presents, in particular for small Hawking temperatures T_{H}, a formidable task [29,30].

Current experiments [25,26] are carried out with flow geometry of strongly elongated condensates, a primary motivation being to avoid turbulence developing when the condensate flows supersonically. Two aspects to be reconciled are of fundamental importance when modeling such black hole analogs, namely what is actually feasible at a laboratory level and what the mathematical complexity of theoretical models requires to be solved. For definiteness, our guiding experimental parameters for system sizes and number of condensed atoms are the ones typically currently implemented in the experiments of [25,26]. In particular, the condensate is radially trapped, operating near a quasi-one-dimensional (quasi-1D) regime. In order to describe the phenomena presented by such quasi-1D analogs, a working hypothesis commonly assumed is the negligibility of the finite axial size of the condensate. When considering the Hawking process, this is usually considered a justified hypothesis if the system boundaries are "sufficiently distant" from the analog event horizon. Due to the inherent complexity of analog black holes in the many-body context of interacting condensates, it is however in general not possible to decide whether or not theoretical models based on the assumption of an infinitely extended quasi-1D condensate correctly capture all features of real finite-size condensates in a controlled manner.

In the following, we employ the idea of using coherent sources [31] to study a finite size quasi-1D analog model containing only a single analog event horizon. Our model assumes the existence of a flowing condensate which is continuously pumped into the system at one of its ends and destroyed at the other, and, arguably, it represents the simplest realizable black hole analog that captures finite size effects without the presence of a white hole. Although being experimentally more intricate than the current implementation of [25,26], the technology needed to sustain such a flowing condensate from condensate reservoirs has been established previously [32–35], the major problem being the reservoir replenishment. Although the latter is necessary for steady-state applications like atom lasers [35,36], the analog model has to operate only for short periods of time until measurements can be performed and replenishment is therefore less crucial than for lasing operation.

For dilute Bose-Einstein condensates (BECs), a quantity of fundamental relevance is quantum depletion, which is a

first-order correlation function. We present below, to the best of our knowledge, the first calculation of depletion in inhomogeneous BECs with a sonic spacetime horizon, to certify whether under certain conditions single-horizon finite-size analog black holes can be prepared in a quasi-1D condensate. We stress that in this regard, most of the current models for 1D analog black holes implement infinitely extended quasicondensates that break the validity of Bogoliubov theory by leading to a depletion diverging with axial system size, a well-known fact for any 1D system to which the f-sum rule can be applied [37]. In our 1D model, depletion is everywhere finite and small for typical black hole parameters throughout the system evolution. We thereby validate the Bogoliubov expansion, which imposes as a prerequisite that depletion must be small.

Although challenging to validate experimentally, that analog Hawking radiation exists is unquestionable by very general arguments [5], and perhaps more important is what analog gravity theory in quantum many-body (condensed-matter) systems can teach us further than predicting the very existence of Hawking radiation *per se*. Of central importance in this regard is how quantum (and thermal) fluctuations created by the Hawking and other processes, propagating on the top of the condensate background backreact on this background, and thus on the motion of the condensate, which in turn affects the production of Hawking radiation. This backreaction can only be described properly within a number-conserving formalism [38], and the determination of quantum depletion is a first necessary step in the complex backreaction program.

The model explored here shares some dynamical features with analog black hole-white hole (BH-WH) systems built from toroidally flowing condensates. Namely, a finite size-induced field dynamical instability develops in such models as well. We therefore review field quantization in the presence of instabilities, which is a well understood topic explored in a plethora of physical contexts, from condensed matter systems [39–41] to cosmology [42,43]. In this context, of particular importance for the Bogoliubov theory is the time-translation-symmetry spontaneous breakdown in stationary condensates by the growing vacuum fluctuations, which prevents the existence of a preferred instantaneous vacuum state. We address this problem by constructing solutions to the Bogoliubov-de Gennes (BdG) equation which takes into account as a starting point of the black hole formation process a well-defined quasiparticle vacuum state.

Describing the dynamical instabilities, our major findings include the simulation of black hole lifetimes as function of experimental parameters, whose intricate functional dependence reveals how strong the correlation of finite size and stability of the black hole is. We also demonstrate the existence of stability regions in parameter space. It is demonstrated that when the sonic horizon just emerges, distinct depletion signatures appear. In particular, we show that the depletion power spectrum changes and new peaks can be detected, which constitutes a valuable tool to identify the emergence of quantum Hawking channels when negligible flux at infinity is present, and the conventional density-density correlation signatures are too weak to be detected by using first-order correlations. Moreover, we show that the radiated signal is correlated with the depletion cloud outside the black hole, and our simulations reveal that the radiative process is accompanied by an increase of the local depletion.

II. THE MODEL

Within the s-wave approximation, the one-dimensional Bose-Einstein condensate under study is described by the action functional ($\hbar = m = 1$)

$$S_c = \int \mathrm{d}^2x\Psi^* \left[i\partial_t + \frac{\partial_x^2}{2} - U_e - \frac{g}{2}|\Psi|^2 \right]\Psi, \qquad (1)$$

where U_e is the external potential. Our goal is to study a black hole model which captures the finiteness of condensates while enabling a fully analytical treatment of the quantum field operator expansion, and which contains as a limiting case an infinite size (quasicondensate) black hole analog. There exists different routes for building such confined flowing condensates. In the experiments of [25,26], a condensate initially at rest is subjected to a moving blue-detuned laser and an analog event horizon is thereby created dynamically. The drawback of this model is that notions of a stationary regime are difficult to establish and a fully numerical analysis is therefore unavoidable. In particular, the moving horizon is responsible for the emergence of an inner horizon, and a BH-WH pair forms [26,30,44]. Different techniques possible to establish analog event horizons include the condensate being released from a reservoir [45] by an outcoupler and the flowing condensate in toroidal configurations [31]; the latter always containing a BH-WH pair, as dictated by the very ring topology.

Before presenting the model, we expand further on why considering configurations of finite extension is important for our analysis instead of the conventionally assumed infinite extension of the system. First of all, Bose-Einstein condensates simply do not exist in infinitely extended quasi-1D black hole models. This can be concluded, for instance, from the condensate perturbations of [46], which imply a (generic) logarithmic divergence of the quantum depletion with the system size at $T = 0$. At finite temperature, this divergence is stronger (linear in system size), as dictated by the Hohenberg theorem [37], showing that finite temperature effects as predicted by quasicondensate models might not be extendable to true condensates. Henceforth, we thus restrict our analysis to zero point (vacuum) fluctuations ($T = 0$), which pertain to the theory sector responsible for the quantum Hawking process. In this

regime, a (weak) logarithmic divergence with the system size means that we can safely consider larger condensates while maintaining sufficient control of the system depletion.

Furthermore, another crucial aspect of infinite size models is linked to the global $U(1)$ symmetry (in the absence of external sources). As the condensate existence breaks this symmetry, the theory always admits at least one zero frequency (Goldstone) excitation, and if the condensate is infinite in size, then the system spectrum is continuous. This is particularly important for black hole analogs, as the Hawking-like process is a low-energy phenomenon, and thus more sensitive to boundary conditions. Accordingly, to assume robustness of the Hawking process with respect to the system size is a rather strong assumption that needs justification. Indeed, the spectrum cannot be continuous for finite size configurations, and because the system is not homogeneous, a nontrivial filtering of the excitations which would exist in infinite analogs should occur.

The strategy pursued in our work, which proposes to realize a finite-size (and therefore well-defined) quasi-1D BEC black hole, consists in building a flowing condensate sustained by continuous coherent sources and drains [31,33] at its boundaries. Mathematically, these are generically modeled by adding to the action (1) a term

$$S_{\mathrm{s}} = \int \mathrm{d}^2x (J_{\mathrm{e}}\Psi^* + J_{\mathrm{e}}^*\Psi), \tag{2}$$

where J_{e} represents the external sources (and drains). Variation of the total action $S_{\mathrm{c}} + S_{\mathrm{s}}$ with respect to Ψ^* leads to the inhomogeneous Gross-Pitaevskii equation [47]

$$\left(-i\partial_t - \frac{\partial_x^2}{2} + U_{\mathrm{e}} + g|\Psi|^2\right)\Psi = J_{\mathrm{e}}. \tag{3}$$

We note that the source field J_{e} is in general complex, and in order to gain insight on its physical meaning we can make use of the Madelung representation $\Psi = \sqrt{\rho}\exp(i\theta)$, where ρ is the condensate density and $v = \partial_x\theta$ the fluid velocity [38]. In terms of the variables ρ and θ, Eq. (3) reads

$$\partial_t\rho + \partial_x(\rho v) = -2\mathrm{Im}[J_{\mathrm{e}}\Psi^*], \tag{4a}$$

$$\partial_t\theta + \frac{v^2}{2} - \frac{\partial_x^2\sqrt{\rho}}{2\sqrt{\rho}} + U_{\mathrm{e}} + g\rho = \frac{\mathrm{Re}[J_{\mathrm{e}}\Psi^*]}{\rho}. \tag{4b}$$

Equation (4a) shows that $-2\mathrm{Im}[J_{\mathrm{e}}\Psi^*]$ is the flux of particles being injected to the system, whereas Eq. (4b) gives rise to an Euler-type equation [38], with an additional term due to the source term of the inhomogeneous Gross-Pitaevskii Eq. (3),

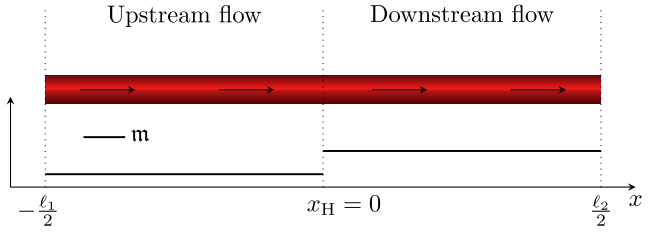

FIG. 1. Schematics of the condensate under study, which is assumed to be a homogeneous quasi-1D condensate of size $(\ell_2 + \ell_1)/2$ flowing at constant velocity. The gas flow is sustained by continuous source and drain at $x = -\ell_1/2$ and $x = \ell_2/2$, respectively. At $x = x_{\mathrm{H}}$, the Mach number $\mathfrak{m}$ has a jumplike discontinuity, separating the system into two regions of different sound velocity.

$$(\partial_t + v\partial_x)v = -\partial_x\left(-\frac{\partial_x^2\sqrt{\rho}}{2\sqrt{\rho}} + U_{\mathrm{e}} + g\rho - \frac{\mathrm{Re}[J_{\mathrm{e}}\Psi^*]}{\rho}\right). \tag{5}$$

The (nonflux) term $\partial_x(\mathrm{Re}[J_{\mathrm{e}}\Psi^*]/\rho)$ therefore acts as an external force density.

Our analog black hole is prepared by adjusting the source field J_{e} and external potential U_{e} such as to produce the profile depicted in Fig. 1. The condensate density ρ is assumed to be constant in condensate support region, and the contact interaction strength g is a piecewise constant function, defined by $g = g_{\mathrm{u}}$ for $x < 0$ and $g = g_{\mathrm{d}}$ for $x > 0$. The resulting background condensate describes a sound barrier thoroughly studied in the literature [27,46,48], where the subscripts "u" and "d" henceforth denote "upstream" and "downstream," respectively. Furthermore, the condensate is trapped inside a 1D box of size $(\ell_2 + \ell_1)/2$ which parametrizes the system finiteness (see Fig. 1).

Now the flowing condensate is modeled by letting $\theta = -\mu t + vx$, where μ is the chemical potential and v is the fluid velocity, both assumed constant. We build the required finite size solution to the system (4) as a limiting process. Let the system density ρ be given by

$$\rho = \begin{cases} \rho_{\mathrm{out}}, & x < -\ell_1/2, \\ \rho_{\mathrm{in}}, & -\ell_1/2 \le x \le \ell_2/2, \\ \rho_{\mathrm{out}}, & \ell_2/2 < x, \end{cases} \tag{6}$$

where ρ_{out}, ρ_{in} are constants, and the external potential is set as

$$U_{\mathrm{e}} = \begin{cases} \gamma\rho_{\mathrm{out}}^{-1/4} + \mu - v^2/2 - g\rho_{\mathrm{out}}, & x < -\ell_1/2, \\ \mu - v^2/2 - g\rho_{\mathrm{in}}, & -\ell_1/2 \le x \le \ell_2/2, \\ \gamma\rho_{\mathrm{out}}^{-1/4} + \mu - v^2/2 - g\rho_{\mathrm{out}}, & \ell_2/2 < x, \end{cases} \tag{7}$$

$\gamma > 0$ being a constant parameter. We use this infinitely extended profile to determine the external source J_{e}, and

then we take $\rho_{\rm out} \to 0$. Notice that in this limit the condensate density is constant inside the box and zero otherwise, whereas the external potential $U_{\rm e}$ gives rise to an infinite square well potential. Returning to Eqs. (4), we thus find the nonflux part of $J_{\rm e}$ to be

$$\frac{\mathrm{Re}[J_{\rm e}\Psi^*]}{\sqrt{\rho}} = \begin{cases} \gamma\rho_{\rm out}^{1/4}, & x < -\ell_1/2, \\ 0, & -\ell_1/2 \le x \le \ell_2/2, \\ \gamma\rho_{\rm out}^{1/4}, & \ell_2/2 < x, \end{cases} + \frac{\sqrt{\rho_{\rm out}} - \sqrt{\rho_{\rm in}}}{2}[\partial_x\delta(x+\ell_1/2) - \partial_x\delta(x-\ell_2/2)], \tag{8}$$

whereas the flux part is given by

$$\mathrm{Im}[J_{\rm e}\Psi^*] = \frac{v(\rho_{\rm out}-\rho_{\rm in})}{2}[\delta(x+\ell_1/2) - \delta(x-\ell_2/2)], \tag{9}$$

and thus ρ, $U_{\rm e}$, and $J_{\rm e}$ given by Eqs. (6), (7), (8), and (9) represent an exact solution to the system (4), with free parameters $\{v, g_{\rm u}, g_{\rm d}, \mu, \ell_1, \ell_2, \rho_{\rm out}, \rho_{\rm in}\}$. Finally, our finite size model is obtained by letting $\rho_{\rm out} \to 0$. In particular, in this limit the external potential becomes

$$U_{\rm e} = \begin{cases} \infty, & x < -\ell_1/2, \\ \mu - v^2/2 - g\rho, & -\ell_1/2 \le x \le \ell_2/2, \\ \infty, & \ell_2/2 < x, \end{cases} \tag{10}$$

where, in order to keep the notation simple, we use henceforth ρ to denote the constant $\rho_{\rm in}$ where it is nonvanishing. We notice also that in this limit the sources and drains are localized: The condensate particles enter the system at $x = -\ell_1/2$ and are absorbed at $x = \ell_2/2$, similar to the external source considered in [47].

The analog model is obtained by studying sound propagation over this condensate solution, i.e., we write $\Psi = \exp(-i\mu t + ivx)(\sqrt{\rho} + \psi)$, where ψ denotes freely propagating small fluctuations. This means that ψ represent linearized solutions ($|\psi|^2 \ll \rho$) to the homogeneous (sourceless) part of Eq. (3)

$$i\partial_t\psi = \left(-\frac{\partial_x^2}{2} - iv\partial_x\right)\psi + g\rho(\psi + \psi^*). \tag{11}$$

Furthermore, due to the infinite square well potential, the wave function is subjected to Dirichlet boundary conditions: $\psi|_{x=-\ell_1/2} = \psi|_{x=\ell_2/2} = 0$ [49].

A relevant quantity that can be constructed from the system parameters is $c = \sqrt{g\rho}$, which has dimensions of velocity, and represents the local sound speed. We say that an analog black hole condensate background *exists* when $v/c_{\rm u} < 1 < v/c_{\rm d}$, or in terms of the Mach number, $\mathfrak{m}_{\rm u} < 1 < \mathfrak{m}_{\rm d}$ (Fig. 1). Thus, we need to specify $\{\mathfrak{m}_{\rm u}, \mathfrak{m}_{\rm d}, \ell_1, \ell_2\}$, to determine the black hole completely. Also, we from now on work in units such that $c_{\rm u} = 1$, which, in addition to the conventional $\hbar = m = 1$, renders the upstream healing length $\xi_{\rm u} = 1/\sqrt{g_{\rm u}\rho}$ to be unity. Finally, canonical quantization is obtained by promoting ψ to an operator-valued distribution $\hat{\psi}$ subjected to equal-time bosonic commutation relations $[\hat{\psi}(t,x), \hat{\psi}^\dagger(t,x')] = \delta(x-x')$. The quantization details are provided in the next section.

III. CANONICAL QUANTIZATION

The procedure to build the quantum field expansion for $\hat{\psi}$ follows the general recipe: Solve for the quasiparticle modes, which constitute a complete set of solutions to the classical field equation. Then, write down the most general classical solution in terms of this complete set and postulate the canonical commutation relations.

A. Quantization

We start by defining the Nambu spinor $\Phi = (\psi, \psi^*)^{\rm t}$, where "t" stands for transpose. Thus, the field equation (11) implies

$$i\sigma_3\partial_t\Phi = \left(-\frac{\partial_x^2}{2} - i\mathfrak{m}_{\rm u}\sigma_3\partial_x + \frac{g}{g_{\rm u}}\sigma_4\right)\Phi, \tag{12}$$

where σ_i, $i = 1,2,3$ denote the usual Pauli matrices, and $\sigma_4 = 1 + \sigma_1$. By definition, the spinor Φ satisfies $\Phi = \sigma_1\Phi^*$, and clearly, upon quantization, we should have

$$[\hat{\Phi}_a(t,x), \hat{\Phi}_b^\dagger(t,x')] = \sigma_{3,ab}\delta(x-x'). \tag{13}$$

Also, from the discussion after Eq. (11), we have that the field Φ is subjected to Dirichlet boundary conditions

$$\Phi|_{x=-\ell_1/2} = 0 = \Phi|_{x=\ell_2/2}. \tag{14}$$

Furthermore, because of the boundary conditions, Eq. (12) implies that if Φ and Φ' are two distinct solutions of the latter equation, then

$$\langle\Phi, \Phi'\rangle = \int \mathrm{d}x\Phi^\dagger(t,x)\sigma_3\Phi'(t,x) \tag{15}$$

is a conserved quantity (in time), which will be used as a scalar product on the space of classical solutions. Also, as the field modes have compact support, they have finite norms, which can be taken in general as

$$\langle\Phi, \Phi\rangle = \pm 1. \tag{16}$$

We stress that even though Eq. (12) may admit nonzero solutions with vanishing norm, we can *always* find an orthonormal basis as in Eq. (16). The plus and minus signs in Eq. (16) correspond to positive and negative norm

modes, and we recall that for each solution Φ of Eq. (12), $\sigma_1\Phi^*$ is also a solution of opposite norm sign. Thus there exists a one-to-one correspondence between positive and negative norm modes, which allows us to index the positive norm solutions as Φ_n, $n = 1, 2, 3, \ldots$. With this, we can write the most general classical solution of Eq. (12) as

$$\Phi(t,x) = \sum_{n=1}^{\infty} [a_n \Phi_n(t,x) + b_n^* \sigma_1 \Phi_n^*(t,x)], \tag{17}$$

and in view of the reflection property $\Phi = \sigma_1\Phi^*$, it follows that $b_n = a_n$. Now, canonical quantization is defined by the promotion of Φ to the operator-valued distribution $\hat{\Phi}$ subjected to the condition (13), which corresponds to promoting each $a_n = \langle \Phi_n, \Phi \rangle$ to an operator $\hat{a}_n$ satisfying

$$[\hat{a}_n, \hat{a}_{n'}^\dagger] = \delta_{n,n'}. \tag{18}$$

Concluding, vacuum states $|0\rangle$ are defined by the kernel condition $\hat{a}_n|0\rangle = 0$, and the full field operator becomes

$$\hat{\Psi}(t,x) = e^{-i\mu t + ivx}[\sqrt{\rho} + \hat{\psi}(t,x)], \tag{19}$$

where $\hat{\psi}$ is the first component of $\hat{\Phi}$. Denoting by $\Phi_n = (f_n, h_n)^{\mathrm{t}}$, we have from Eq. (17)

$$\hat{\psi}(t,x) = \sum_{n=1}^{\infty} [\hat{a}_n f_n(t,x) + \hat{a}_n^\dagger h_n^*(t,x)]. \tag{20}$$

B. Field modes in the presence of a black hole

Because the system is stationary *at the classical level*, solutions to the field equation can be found in the form $\Phi(t,x) = \exp(-i\omega t)\Phi_\omega(x)$, and if Φ_ω is a solution associated to ω, then $\sigma_1\Phi_\omega^*$ is also a solution, associated to $-\omega^*$. In this way, we exhaust all real frequencies in the system spectrum by focusing on $\omega > 0$ only. Moreover, we say that the system is unstable if there exists a solution with $\mathrm{Im}[\omega] > 0$. For each such solution, the spectrum necessarily contains also the frequency ω^*, as guaranteed by the hermiticity of the Hamiltonian [39]. Thus, we need to solve

$$\omega\sigma_3\Phi_\omega = \left(-\frac{\partial_x^2}{2} - i\mathfrak{m}_{\mathrm{u}}\sigma_3\partial_x + \frac{g}{g_{\mathrm{u}}}\sigma_4\right)\Phi_\omega, \tag{21}$$

for $\mathrm{Re}[\omega] \geq 0, \mathrm{Im}[\omega] \geq 0$, and where each Fourier component $\Phi_\omega(x)$ is subjected to Eq. (14). Furthermore, wave mechanics techniques [50] applied to Eq. (21) imply that Φ_ω and its first derivative are also continuous at $x = 0$. These two conditions, plus the other two in Eq. (14) give a total of eight constraints that each field mode must satisfy.

For $x \neq 0, -\ell_1/2$, and $\ell_2/2$, the general solution of the ordinary differential equation (21) is a combination of exponentials of the form $\exp(ikx)\zeta_k$, for constant ζ_k,

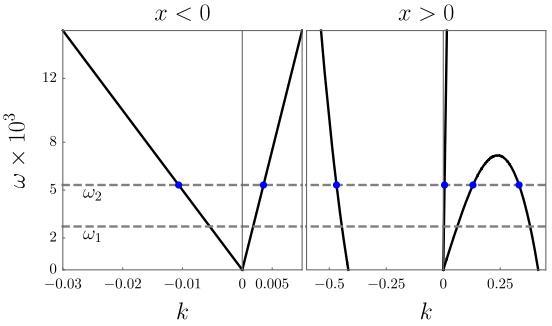

FIG. 2. Bogoliubov dispersion relation $\omega = \omega(k)$ for real k, from Eq. (22). We set $\mathfrak{m}_{\mathrm{u}} = 0.5$, $\mathfrak{m}_{\mathrm{d}} = 1.1$, or $g_{\mathrm{d}}/g_{\mathrm{u}} \sim 0.2$. Left: Dispersion relation in the region $x < 0$. The gray dashed lines correspond to the two discrete eigenfrequencies of our finite system which are located within the ω range shown, for a condensate with $-\ell_1/2 = \ell_2/2 = 60$. The blue points indicate the solutions for ω_2. Right: Dispersion relation for the region $x > 0$. Because $\mathfrak{m}_{\mathrm{d}} > 1$, the negative branch of the dispersion relation presents a local maximum. We note that the field modes ω_1 and ω_2 are below this local maximum.

which, upon substitution in Eq. (21) results in the familiar Bogoliubov dispersion relation

$$(\omega - \mathfrak{m}_{\mathrm{u}}k)^2 = k^2\left(\frac{g}{g_{\mathrm{u}}} + \frac{k^2}{4}\right). \tag{22}$$

Notice that for each value of ω, this equation, being a fourth-order polynomial equation in k, always has four solutions (not necessarily distinct), as shown diagrammatically in Fig. 2. For simplicity, we shall denote by p the downstream solutions, and thus the general solution for Φ_ω has the form

$$\Phi_\omega = \begin{cases} \sum_p s_p e^{ipx}\zeta_p, & x > 0, \\ \sum_k s_k e^{ikx}\zeta_k, & x < 0, \end{cases} \tag{23}$$

where the various coefficients s_k and s_p are integration constants, and

$$\zeta_k = \begin{pmatrix} g/g_{\mathrm{u}} \\ \omega - \mathfrak{m}_{\mathrm{u}}k - k^2/2 - g/g_{\mathrm{u}} \end{pmatrix}. \tag{24}$$

For each possible field mode, clearly at least one of the coefficients s_k, s_p is nonzero, which can then be taken as a normalization constant. This means that a total of seven conditions are necessary and sufficient to fix the integration constants, which can be done in a straightforward manner by using seven of the eight boundary conditions. The remaining equation thus becomes an analytical function of ω through the roots k, p, and the s_k and s_p, which determines the ω frequencies which are contained in the

system spectrum. Furthermore, because the remaining equation is analytic in ω, the spectrum is discrete. Therefore, the recipe just presented exhausts all possible field modes, which can then be normalized and added to the field expansion of Eq. (17).

IV. BLACK HOLE LIFETIMES

As in any experimental realization of a trapped BEC, the system confinement implies that small disturbances propagating over the BEC also stay trapped throughout the system evolution. In our analog model, this property is captured by the Dirichlet boundary conditions (14) at the system (hard) walls, which are a particular way of modeling perfect mirrors for the system radiation. Therefore, considerable differences as regards the predictions of finite size and infinitely extended analog black hole models are expected to occur, for during the black hole existence the energy (continuously) extracted from the background by the Hawking-like process is not allowed to radiate away in the finite size model and stays contained within the hard-walled box, i.e., the condensate can in principle act as a resonant cavity for the sound waves. This characteristic, however, does not necessarily lead to *dynamical instabilities*, i.e., complex frequencies in the system spectrum. In fact, analog models containing BH-WH pairs usually present a black hole lasing effect [13], but in [31] the authors also found dynamically stable configurations in BH-WH analogs in toroidal (and thus finite size) condensates.

It is noteworthy that because of the complexity of BH-WH analogs, the mechanisms leading to stabilization cannot in general be easily disentangled from one another [51,52]. In our single black hole analog model a similar interplay between the system finite size and the radiation process is observed, which leads to dynamically stable or unstable configurations rather sensitively depending on the system parameters, revealing that finite size effects play a prominent role in the (de)stabilization of analog black holes in BECs.

In dynamically unstable scenarios, a natural notion is therefore that of black hole lifetime, as determined by the instability time scale. We note in this regard that previously the instability of BH-WH configurations was explored for instance in [31,53,54]. The authors studied the instability dependence as function of the system parameters. More recently, such an analysis has been pursued in [55] for a (more realistic) quasicondensate configuration.

In principle, the system spectrum, which contains the complex frequencies, depends solely on the condensate configuration, and thus the involved instability time scales are uniquely determined *as long as the condensate exists in that state*, i.e., as long as quantum fluctuations remain small. Therefore, by ensuring that we always start from a scenario of well-defined quantum fluctuations (e.g., by determining the condensate depletion), the unstable frequencies set the time scales for the black hole existence which we study in this section.

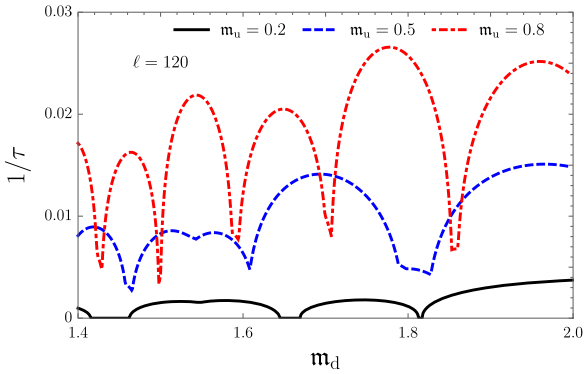

FIG. 3. Black hole lifetimes as function of the downstream Mach number $\mathfrak{m}_{\rm d}$ for several choices of $\mathfrak{m}_{\rm u}$. Here we set $\ell = 120$. Notice that generally no monotonic behavior is observed. Moreover, the lifetimes diverge ($1/\tau = 0$) for $\mathfrak{m}_{\rm u} = 0.2$ and some values of $\mathfrak{m}_{\rm d}$, i.e., the black continuous curve then touches the $\mathfrak{m}_{\rm d}$ axis.

Four parameters are necessary to specify the analog black hole: $\{\mathfrak{m}_{\rm u}, \mathfrak{m}_{\rm d}, \ell_1, \ell_2\}$. For the sake of simplicity, let us assume that one fixes $\ell_1 = \ell_2 = \ell$. We define the *analog black hole lifetime* generally as

$$\tau = \min_{\omega\in\Sigma}(2\mathrm{Im}[\omega])^{-1}, \tag{25}$$

where Σ is the subset of mode frequencies ω in the Bogoliubov spectrum with $\mathrm{Im}[\omega] \geq 0$. We can study the lifetimes as function of the three free parameters. For instance, in Fig. 3 we plot $1/\tau$ as functions of the downstream Mach number for several upstream Mach numbers. From the figure, the remarkable effect of the finite system size on the Hawking process can be clearly seen. For an infinite system $\ell_1 = \ell_2 \to \infty$, no dynamical instability exists, and the black hole lifetime is formally infinite, although of course the condensate is destroyed by phase fluctuations and is completely depleted [37]. On the other hand, when the system has finite size, no monotonic behavior as a function of the Mach numbers is observed. Even more noteworthy is the existence of stability regions, which from Fig. 3 appear for the parameters $\mathfrak{m}_{\rm u} = 0.2$, $\ell = 120$ (the black continuous curve) where the lifetime diverges. For these parameters, as discussed in the above, there exists a compensation between different mechanisms in the system, that therefore becomes dynamically stable.

In Fig. 4, we depict the lifetimes as a function of the system size. Again, no clear functional dependence with the system parameters can be inferred, a feature also observed in the BH-WH calculations of [31,53–55]. We note, however, that the complex dependence of τ with $\{\mathfrak{m}_{\rm u}, \mathfrak{m}_{\rm d}, \ell\}$ is expected because each field mode is built by combining the eight distinct channels solutions of

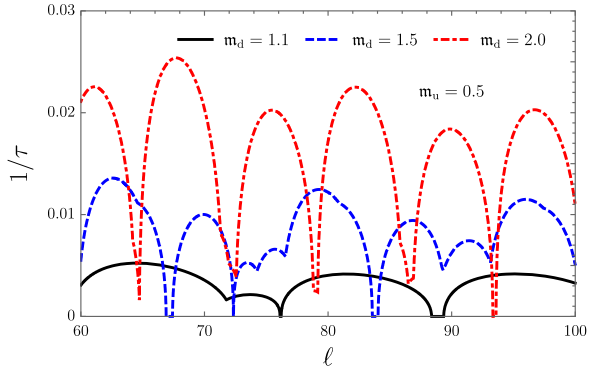

FIG. 4. Black hole lifetimes as function of the system size for the fixed upstream Mach number $\mathfrak{m}_u = 0.5$ and several choices of $\mathfrak{m}_d$. Similarly to what is observed in Fig. 3, there is no clear functional dependence of the lifetimes on the system size, and stability regions in the space of parameters exist.

Eq. (22) and the eight boundary conditions discussed in Sec. III B.

V. THE SYSTEM VACUUM STATE IN THE PRESENCE OF INSTABILITIES

Field quantization in the presence of instabilities is a well-studied topic [39–43], and the canonical procedure of Sec. III also in such a case works in general. For our particular goal of simulating quantum depletion, a major aspect of this particular brand of quantization is the notion of an instantaneous vacuum state, a state such that $\langle\hat{\psi}\rangle = 0$. As pointed out in [40], the presence of instabilities during the black hole existence prevents the selection of a preferred instantaneous vacuum state, which in stationary configurations, as the name suggests, can be chosen with respect to the laboratory frame via a complete set of normalizable solutions whose positive norm field modes Φ_n are stationary (eigenfunctions) with respect to the generator of time translations $i\partial_t$. In this work we refer to this vacuum state as the quasiparticle vacuum. Notwithstanding, in the presence of instabilities, the operator $i\partial_t$ has non-normalizable eigenfunctions with complex eigenvalues. Thus, bona fide normalizable positive norm field modes constructed from non-normalizable eigenfunctions cannot be eigenfunctions of $i\partial_t$, and in this case we say that quantization spontaneously breaks the time translation symmetry of the theory, and hence no quasiparticle (preferred) vacuum exists. We quote [20] for further details regarding the quasiparticle vacuum in infinitely extended 1D quasicondensate analogs.

In order to highlight the issues with fixing an instantaneous vacuum during an unstable black hole evolution, let Ω, Ω^* be one of the complex frequency pairs in the spectrum, and let the corresponding solutions to Eq. (12) be $\exp(-i\Omega t)\Phi_\Omega(x)$ and $\exp(-i\Omega^* t)\Phi_{\Omega^*}(x)$, respectively. Thus, it follows from the time independence of Eq. (15) and $\mathrm{Im}[\Omega] > 0$ that these two solutions have zero norm, but $\langle\Phi_\Omega, \Phi_{\Omega^*}\rangle := \lambda\exp(i\theta) \neq 0$, in such a way that the two combinations

$$\Phi^{(+)}_{\Omega,\alpha\beta} = \frac{\alpha}{\sqrt{\lambda}}\left[e^{-i\Omega t}\Phi_\Omega + \left(\frac{1}{2\alpha^2} + i\beta\right)e^{-i\theta - i\Omega^* t}\Phi_{\Omega^*}\right], \quad (26)$$

$$\Phi^{(-)}_{\Omega,\alpha\beta} = \frac{\alpha}{\sqrt{\lambda}}\left[e^{-i\Omega t}\Phi_\Omega - \left(\frac{1}{2\alpha^2} - i\beta\right)e^{-i\theta - i\Omega^* t}\Phi_{\Omega^*}\right], \quad (27)$$

for $\alpha > 0$ and real β are orthonormal, with $\Phi^{(+)}_{\Omega,\alpha\beta}$ (respectively $\Phi^{(-)}_{\Omega,\alpha\beta}$) being a positive (respectively negative) norm solution. If Ω lies on the imaginary axis, we can add $\Phi^{(+)}_{\Omega,\alpha\beta}$ and $\sigma_1\Phi^{(+)*}_{\Omega,\alpha\beta}$ as a positive-negative norm pair of field modes to the field expansion, whereas if Ω is not on the imaginary axis, we must add $\Phi^{(+)}_{\Omega,\alpha\beta}$ and $\sigma_1\Phi^{(-)*}_{\Omega,\alpha\beta}$ and the corresponding negative norm counterparts to the expansion. Now, inspection of the modes (26) and (27) reveals that each choice of (α, β) is equally acceptable, and it gives rise to a distinct quantum field theory as can be seen by determining the Bogoliubov transformation between the different sets of modes. In particular, we note that it is, in principle, possible that the vacuum state under study represents a strongly-depleted condensate, rendering the whole Bogoliubov expansion inconsistent. We shall return to this question in the next section when we discuss condensate depletion.

A. Quenching to a black hole

An elegant way of fixing a preferred vacuum state if the analog is dynamically unstable is provided by the fact that amongst the various condensate configurations included in our analysis, there are stationary configurations which can be used as initial conditions before quenching to the final black hole configuration. For instance, we can start from a system for which, at $t < 0$, both Mach numbers $\mathfrak{m}_u$, $\mathfrak{m}_d$ are smaller than 1, and at $t = 0$, the coupling g_d is adjusted to set $\mathfrak{m}_d > 1$ to the required value to create the sonic horizon. In this way, as we work in the Heisenberg picture, the initial stationary vacuum remains well-defined throughout the system evolution. Specifically, the quantum field $\hat{\Phi}$ has the general expansion of Eq. (17), where all functions $\Phi_n(t, x)$ have positive norm and are solutions of the BdG equation at all times, such that for $t < 0$,

$$\Phi_n(t, x) = e^{-i\nu_n t}\Phi_{\nu_n}(x), \quad (28)$$

$\nu_n > 0$ for all n. Accordingly, because of the quench, the field mode $\Phi_n(t, x)$ after $t = 0$ can be expanded in terms of any complete set of solutions, i.e.,

$$\Phi_n = \sum_{m=1}^{\infty} [\alpha_{n,m} e^{-i\omega_m t}\Phi_{\omega_m} + \beta_{n,m} e^{i\omega_m t}\sigma_1 \Phi^*_{\omega_m}] + \sum_j \gamma_{n,j} e^{-i\Omega_j t}\Phi_{\Omega_j}, \tag{29}$$

and the sum in j runs over all complex frequency solutions. Returning to the BdG equation, we conclude from the term $i\partial_t\Phi_n$ that $\Phi_n(t,x)$ is continuous at $t=0$, which amounts to the Fourier expansion

$$\sum_{m=1}^{\infty} [\alpha_{n,m}\Phi_{\omega_m} + \beta_{n,m}\sigma_1\Phi^*_{\omega_m}] + \sum_j \gamma_{n,j}\Phi_{\Omega_j} = \Phi_{\nu_n}. \tag{30}$$

Thus by projecting this equation onto the direction of the field modes the matrices $\alpha_{n,m}$, $\beta_{n,m}$, and $\gamma_{n,j}$ are uniquely fixed, i.e., the solution to the BdG equation is fixed. By using this quantum field expansion instead of the instantaneous quantization when already residing within the unstable phase, the vacuum state is defined to be the quasiparticle vacuum $\hat{a}_n|0\rangle = 0$, which has a clear interpretation as it is uniquely defined.

VI. QUANTUM DEPLETION AND THE VALIDITY OF THE BOGOLIUBOV EXPANSION

With the aid of the quantum field expansion, we are able to compute quantum depletion, defined as the vacuum expectation value $\delta\rho = \langle\hat{\psi}^\dagger\hat{\psi}\rangle$. The interpretation of quantum depletion is that even at $T=0$, a finite fraction of the condensed particles leaves the condensate due to the inherent quantum fluctuations caused by the interaction of the particles constituting the system [56]. Thus, this *measurable* quantity represents a fundamental tool in the theory of Bose-Einstein condensation. Its knowledge is necessary to validate the Bogoliubov expansion, as the ratio depleted/condensed particles should be small for the very expansion implemented in [Eq. (19)] to be consistent.

Different upper bounds for the Bogoliubov expansion applicability can be adopted, depending on the characteristics of each particular system. For instance, the simulations that follow are such that the largest number of depleted particles occurs near the analog event horizon, roughly when (reinstating units for clarity) $\xi_u\delta\rho \sim 2$. For a condensate which has $\xi_u\rho \sim 60$, this corresponds to 3% of depleted particles near the event horizon. In the present work we fix, by convention, that the Bogoliubov theory predictions are considered to be accurate as long as depletion remains below 10%.

Based on the discussion of Sec. III, we use Eq. (20) to write the depletion as

$$\delta\rho(t,x) = \sum_{n=1}^{\infty} |h_n(t,x)|^2. \tag{31}$$

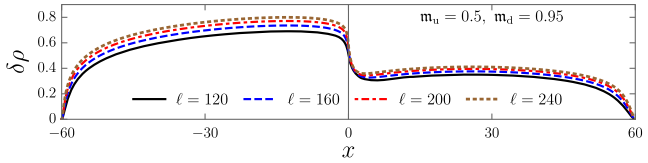

FIG. 5. Quantum depletion for several condensate sizes in the absence of a black hole $\mathfrak{m}_d = 0.95$. Here, $\ell_1 = \ell_2$, and we recall that $\ell \equiv (\ell_2 + \ell_1)/2$. The curves are scaled in x to fit in the same plot. The effect of the system size is to increase the overall depletion logarithmically.

A. Depletion before the black hole formation

From Eq. (31), depletion can be calculated in a straightforward manner using the field modes constructed in Sec. III B, and we expect a logarithmic divergence with system size (see also for instance [46]). We thus expect to see an overall increase in depletion as the system size grows, and we verified this to occur already *before the black hole exists*, as shown in Fig. 5. Other notable features revealed by the plots in Fig. 5 include their shape robustness as the system size grows, the smaller number of depleted particles at the downstream region, caused by the fact that $g_d < g_u$ (weaker particle interactions), and the decrease in the number of depleted particles near the condensate boundaries. This latter aspect comes from the particular form of the chosen external potential, which is set such as to impose Dirichlet boundary conditions. From the plot, we can assess that this form of potential results in a vanishing depletion at the condensate walls, a behavior not expected if the system were prepared with a different external potential.

B. Depletion of a stationary black hole

When the black hole is formed, the depletion curves are qualitatively distinct, and let us consider first quantum depletion in stationary (dynamically-stable) black hole configurations. We present in Fig. 6 our findings for a

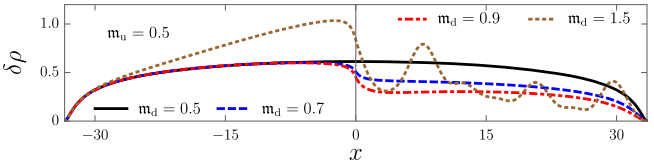

FIG. 6. Several depletion profiles for fixed $\mathfrak{m}_u = 0.5$, and $\ell = 67$. The continuous black, dashed blue, and dot-dashed red curves correspond, respectively, to $\mathfrak{m}_d = 0.5$, $\mathfrak{m}_d = 0.7$, and $\mathfrak{m}_d = 0.9$, whereas the dotted brown curve depicts depletion for the stationary, stable configuration with $\mathfrak{m}_d = 1.5$. Deep into the upstream region we see that the sound barrier at $x = 0$ leaves no imprint in the black hole's absence, but as the analog event horizon forms, the upstream noncondensed cloud changes due to the analog black hole Hawking radiation. We also note the intricate depletion behavior at the downstream region after the black hole formation, which is in sharp distinction to the featureless depletion profile without black hole.

stationary black hole analog defined by $\mathfrak{m}_u = 0.5$, $\mathfrak{m}_d = 1.5$, $\ell = 67$, which, from Fig. 4, can indeed be seen to correspond to a divergent lifetime. Figure 6, which represents one of our major findings, depicts how the upstream noncondensed cloud outside the black hole ($x < 0$) is affected by the Hawking-like radiation. We also plot depletion profiles for a fixed upstream Mach number $\mathfrak{m}_u = 0.5$ and different $\mathfrak{m}_d < 1$. The latter reinforces the intuition in the absence of a black hole, a variable g at $x = 0$ models a sound barrier for the phonon field that should not be perceived far away from the barrier ($|x| \gg 1$). The continuous, dashed, and dot-dashed curves in Fig. 6 show that in the black hole's absence, depletion is indeed only locally affected by the sound barrier; it is not possible to detect its presence by measurements of the depleted cloud if $|x| \gg 1$. However, after the black hole is formed, a clear contribution to depletion deep into the upstream region appears.

It is possible to directly correlate the imprint on the upstream noncondensed cloud far from the analog event horizon to the Hawking-like radiation if we assume that the condensate is extremely elongated, by using, for instance, the field modes of [46]. Such a calculation, however, requires the use of frequency cutoffs to render depletion finite in our quasi-1D setup; such cutoffs can be inferred from our finite size model. We notice also from Fig. 6 the intricate equilibrium pattern displayed by the depleted cloud in the downstream region.

Density modulations similar to the ones found in Fig. 6 can occur in certain inhomogeneous supersonic flows due to the Bogoliubov-Cherenkov-Landau (BCL) radiation phenomenon [57], as reported recently in the analog black hole experiment of [26]. We can however rule out BCL radiation in our setup. The characteristic feature of the BCL mode is that it represents a zero frequency excitation [44]. There is, though, no such zero frequency mode present in our system, as it is sustained by external source and drain, which prevents the condensate phase diffusion in a finite size system, associated with a zero frequency mode [58].

We also note that the various possible sources of depletion, in the sum in Eq. (31), cannot be disentangled in an obvious manner, and thus it is not clear how to determine (in a controlled way) the dependence of the interference pattern in Fig. 6 on the system parameters.

C. Depletion after the formation of an unstable black hole

We now discuss how to probe the event horizon existence by measurements of the downstream depleted cloud in the most common case of analogs that can be studied with our confined system; dynamically unstable black holes. When an analog black hole has just formed, and a phonon field instability then develops, we expect to see a continuous extraction of atoms from the condensate (depletion increase), and the whole system will eventually assume a new configuration. Naturally, to determine how the system will ultimately stabilize and to describe the nature of the final state, a fully self-consistent backreaction analysis is required, which is beyond the scope of this work. Nevertheless, the instability onset can be explored with our quantization scheme, and this subsection is dedicated to such an analysis.

As discussed in Sec. V, in the absence of a stationary regime in unstable scenarios, we need to specify initial conditions for the system, and for the sake of illustration, let us therefore start by considering an instantaneous vacuum state for the phonon field when the black hole is already formed. Note that even if the unstable modes possess negligible absolute frequencies, it is not in general possible to treat the system as an effectively stable one due to the breakdown of time translation symmetry (see in this regard Sec. V).

In order to gain further insight, we shall treat an explicit example thoroughly. Consider the case where $\mathfrak{m}_u = 0.5$, $\mathfrak{m}_d = 1.1$, and $\ell_1 = \ell_2 = 120$, which corresponds to a condensate of total size $\ell = 120$. The perturbation spectrum for this configuration contains exactly six complex frequencies, obtained from $\Omega_1 \sim i8 \times 10^{-4}$ and $\Omega_2 \sim (70.76 + 3i) \times 10^{-4}$. Therefore, from the discussion that leads to Eqs. (26) and (27), we see that the space of possible choices for the system vacuum is parametrized by four real parameters, two for each complex frequency in the upper right portion of the complex plane. For each vacuum state, the sum in Eq. (31) splits into a time-dependent contribution to the system depletion (which contains the unstable field modes), and a time-independent part denoted by $\delta\rho_s$, the latter also being independent of the vacuum choice. Following the notation of Eqs. (20), (26), and (27), the depletion assumes the form

$$\delta\rho = \delta\rho_s + |h^{(+)}_{\Omega_1,\alpha\beta}|^2 + |h^{(+)}_{\Omega_2,\alpha'\beta'}|^2 + |f^{(-)}_{\Omega_2,\alpha'\beta'}|^2, \quad (32)$$

where $\alpha > 0, \alpha' > 0$, β, β' are *any* real parameters. The importance of this result for our analysis is that however large the time scale imposed by the instability for the condensate depletion is, it is in principle possible that no vacuum state exists for which $\delta\rho \ll \rho$, rendering the whole quantization procedure based on the Bogoliubov expansion inconsistent. We can visualize this by counting the total number of depleted particles, $\delta N = \int dx \delta\rho$, which in view of Eq. (32) splits into a contribution from the stable modes, a contribution from the sector Ω_1, and one from the sector Ω_2. We plot in Fig. 7 the number of depleted particles due to the unstable modes from the sector Ω_2 for different choices of initial states parametrized by α', β'.

Inspection of Fig. 7 reveals that depending on the parameters α', β', the predictions of Bogoliubov theory can not be expected to be completely reliable. For instance, for a system with a total of 6000 particles, 1000 depleted particles corresponds to 16% of the particles not in the

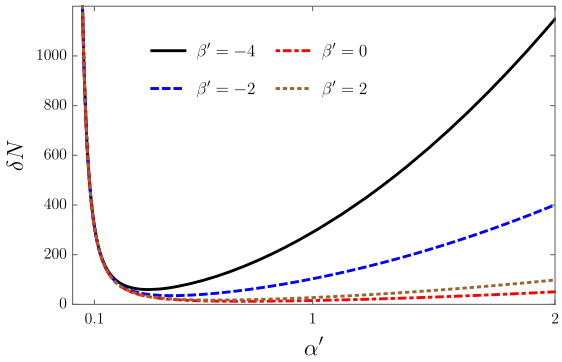

FIG. 7. Quantum-depleted number of particles coming from different choices of instantaneous vacuum states for the sector Ω_2. System parameters are $\mathfrak{m}_u = 0.5$, $\mathfrak{m}_u = 1.1$, and $\ell = 120$.

condensate. This violates the small depletion criterion of the Bogoliubov expansion, and it is thus not possible to decide whether the quantization is consistent, or even if the corrections to the condensate remain negligible. A regime of "initially" large depletion corresponds to cases where the instability already played a relevant role, and de-stabilization processes are taking over the condensate evolution.

On the other hand, as the number of depleted particles is bounded from below, there must exist a vacuum state which renders the smallest depletion, as the Fig. 7 suggests. It is straightforward to show, by minimizing the total number of depleted particles with respect to the parameters $\alpha, \alpha', \beta, \beta'$, that there is only one possible choice for the minimizer, which is depicted in Fig. 8. This result presents a sharp lower bound for depletion in our black hole analog.

The problem of identifying a vacuum state during the unstable phase usually restricts the applicability of the theory to the study of asymptotic regimes, at late times, and as shown here, in the presence of condensates, the analysis is further complicated by whether the condensate persists against quantum depletion. This problem is however of theoretical importance only, as it comes from the assumption that the system is stationary, and everlasting, even though spontaneously growing quantum fluctuations

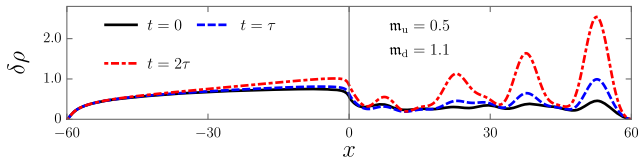

FIG. 8. Depletion profiles as function of time for a black hole characterized by $\mathfrak{m}_u = 0.5$, $\mathfrak{m}_d = 1.1$, and $\ell = 120$, with the system in its vacuum state of minimum depletion. Three major features are observed: Initially (black curve), the depletion profile inside the black hole does not resemble the stable curves of Fig. 5; as time passes, the number of depleted particles increases outside the black hole; an oscillatory pattern emerges inside the black hole. Here, the lifetime τ is defined in (25).

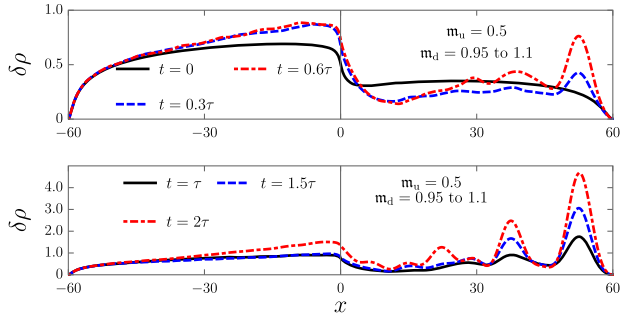

FIG. 9. Depletion profiles as function of time for a quenched black hole. The system is set to have $\mathfrak{m}_u = 0.5$, $\mathfrak{m}_d = 0.95$, and $\ell = 120$ for $t < 0$, and we change $\mathfrak{m}_d = 1.1$ after the quench at $t = 0$.

break the time translation symmetry. In experimental realizations, the condensate and the black hole setting must have a starting point, which defines the system vacuum (and therefore the condensate) throughout its evolution. This is captured by the quench described in Sec. V A, which we explore now.

Still assuming the model with $\mathfrak{m}_u = 0.5$, and $\ell_1 = \ell_2 = 120$, let us consider the case for which at $t = 0$, the system passes from $\mathfrak{m}_d = 0.95$ (the continuous line in Fig. 5) to $\mathfrak{m}_d = 1.1$. In this case, the lifetime τ for the system is set by Ω_1, which has the larger imaginary part. By using Ref. [25] and its experimental parameters as a guide, and returning to dimensionful units, we find $\tau \approx 8$ s for a chemical potential of 70 Hz. We plot in Fig. 9 our findings for this quenched system.

As advocated in the above, by starting from a truly stationary system in its uniquely defined quasiparticle vacuum, we can study the system evolution in a consistent and self-contained way when the Hawking process is switched on. Inspection of Fig. 9 reveals that as the black hole forms, a nontrivial quantum depletion response is triggered, with the formation of an interference pattern inside the black hole (downstream region) and the continuous increase of the overall number of depleted particles, inside and outside the black hole. For this model, $\mathfrak{m}_d$ is increased by decreasing the particle interaction strength g_d, which in stable nonblack hole configurations diminishes the local condensate depletion, as we can see by comparing the upstream and downstream density profiles of Fig. 5. However, the curves in Fig. 9 show that this dependence is not observed in general when $\mathfrak{m}_d$ exceeds 1 and the black hole is formed. We furthermore call attention to the depletion profile outside the black hole, where we see the emergence of the depletion signal discussed in Sec. VI B.

We can follow the ramp-up of the Hawking radiation with a better resolution by taking analog models with higher downstream Mach numbers, which corresponds to stronger radiation [46]. For the sake of illustration, simulations are depicted in Fig. 10 for the Mach numbers $\mathfrak{m}_u = 0.5$, $\mathfrak{m}_d = 2$.

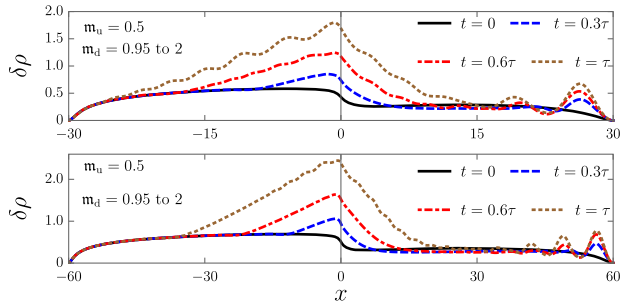

FIG. 10. Quantum depletion for quenched black holes of different sizes. The black holes have $\mathfrak{m}_u = 0.5$, and the quench changes $\mathfrak{m}_d$ from 0.95 to 2 at $t = 0$. The increased downstream Mach number leads to a stronger radiation [46]. Upper panel: $\ell = 60$. Lower panel: $\ell = 120$. Both systems present similar depletion behavior, with the emergence of an oscillatory pattern inside the black hole, and the peculiar upstream-depleted cloud signal discussed in Sec. VI B, which forms at the analog event horizon ($x = 0$) and then propagates against the condensate flow.

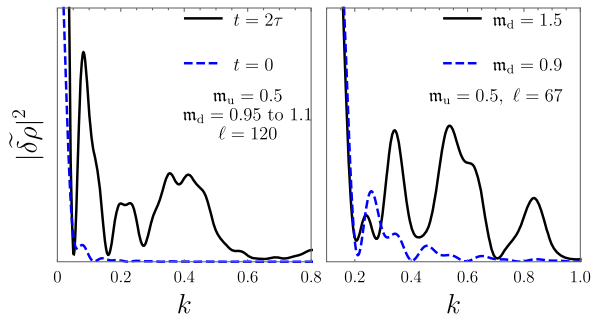

FIG. 11. Power spectrum of the depletion profile for two black hole analogs. Left panel: The two curves represent the observed spectrum at different instants of time for an unstable black hole configuration, both at the beginning of the quench, and after a time $t = 2\tau$, for a black hole characterized by $\mathfrak{m}_u = 0.5$, $\ell = 120$, and $\mathfrak{m}_d = 0.95$ for $t < 0$, $\mathfrak{m}_d = 1.1$, $t > 0$. The black continuous curve shows the formation of a bump near $k \sim 0.4$, absent before the black hole forms, as indicated by the blue dashed curve. Right panel: Power spectrum for the stable black hole (continuous black curve) of Fig. 6. The blue dashed curve shows the power spectrum before the black hole formation.

We obtain a lifetime, cf. Eq. (25), of $\tau \sim 1$ s for a system of total size $\ell = 120$ and chemical potential 70 Hz, about ten times smaller than the one found for the system in Fig. 9 with $\mathfrak{m}_d = 1.1$. Furthermore, $\tau \sim 0.7$ s for a size $\ell = 60$. Figure 10 shows that, as the Hawking-like process is switched on, the cloud of depleted particles increases in a manner directly correlated to the radiated signal. The depleted cloud in a fixed upstream region only responds to the radiation as it reaches that region, and as time passes, because the system is out of equilibrium, the number of depleted particles increases gradually until Bogoliubov theory is no longer reliable. Furthermore, although this depletion response to the radiation sheds some light onto the system evolution, it does not uniquely fix how the background condensate changes, i.e., how backreaction takes place, for whose consistent description a number-conserving analysis is required.

D. Power spectrum of quantum depletion

As a particularly noteworthy feature, our analysis reveals the possibility of probing the existence of an analog event horizon from the emergent interference pattern manifest in the local quantum depletion using the Bragg technique employed by [59]. Denoting Fourier transforms as $\tilde{\rho}(k) = \int \mathrm{d}x \exp(-ikx)\rho(x)$, and similarly for $\widetilde{\delta\rho}(k)$, Ref. [59] exploits the fact that in some configurations $\tilde{\rho}(k)$ decays faster for large k in comparison to the polynomial decay of $\widetilde{\delta\rho}(k)$. One thus obtains a large k window which is sensitive to depletion. The emergence of the interference pattern in Fig. 9 upon formation of the horizon transforms to distinct peaks in $\tilde{\rho}(k)$, as shown for two black hole examples in Fig. 11.

Finally, as already discussed in Sec. VI B above, a unique physical mechanism for the oscillations observed in the depletion profile of the stationary black hole analog of Fig. 6 cannot be clearly identified. In particular, we observe that there is no evident relation between what would correspond to a BCL wave vector ($k \sim 0.75$) solution of Eq. (22) and the peak positions in Fig. 11 right panel, thus also from this point of view ruling out BCL radiation as a source of the oscillations.

On the other hand, for the quenched unstable black holes, the depletion is asymptotically, at late times, dominated by the unstable field modes, which then determine the peaks in the depletion power spectrum (see Fig. 11 left panel).

VII. SUMMARY AND FINAL REMARKS

We proposed a finite size quasi-1D analog black hole model which contains a single event horizon. The model is possibly the simplest one that encapsulates such a single horizon and enforces zero vacuum fluctuations (Dirichlet boundary conditions) at the condensate walls. We note that other boundary conditions can also be used, as for instance Neumann conditions. However, Dirichlet conditions are better suited when we take into account that in experimental realizations the condensate is subject to confining potentials along its symmetry axis. Furthermore, the main advantage of adopting a finite size condensate is that it allows for a controlled usage of Bogoliubov theory by rendering quantum depletion finite and well-defined in a quasi-1D system.

We demonstrate the existence of finite-size-induced dynamical instabilities for the majority of the black hole analogs we probe. By reviewing canonical field quantization in the presence of instabilities, we show that if the phonon field is not carefully quantized, the theory can represent a strongly depleted condensate, which renders the

Bogoliubov expansion inconsistent. We addressed this problem by employing a quenching from a stationary configuration in its quasiparticle vacuum to the final black hole under study. This procedure enabled us to simulate the evolution of the depletion cloud during the instability onset. We found that two distinct signatures of the Hawking process emerge when the event horizon forms, the first one being the appearance of an oscillatory pattern in the depletion cloud inside the black hole which translates to distinct peaks in its power spectrum. As a second feature, the quench we impose reveals the existence of a link between the radiation emitted by the black hole and the depletion cloud, namely, the local depletion at a region outside the black hole starts to increase as the radiation reaches that region. This represents a novel signature of the Hawking radiation ramp-up that is related to the overall distribution of particles either belonging to the condensed or noncondensed part of the system.

We finally comment on the relevance of our results for real black holes. In analog gravity, the quantum many-body wave function of the whole system can (in principle) be accessed via the observer in the lab. Similarly, we anticipate that while in the currently existing nonunified theory of quantized matter fields propagating in a classical, fixed curved spacetime background, the depletion oscillations are hidden behind the horizon, a unitary closed system evolution, potentially provided by a future unification of gravity with the matter fields, will effectively provide access to the black hole quantum interior and thus also to the depletion oscillations we have investigated.

ACKNOWLEDGMENTS

This work has been supported by the National Research Foundation of Korea under Grants No. 2017R1A2A2A05001422 and No. 2020R1A2C2008103.

[1] S. W. Hawking, Black hole explosions?, Nature (London) **248**, 30 (1974).
[2] S. W. Hawking, Particle creation by black holes, Commun. Math. Phys. **43**, 199 (1975).
[3] S. B. Giddings, Black holes in the quantum universe, Phil. Trans. R. Soc. A **377**, 20190029 (2019).
[4] W. G. Unruh, Experimental Black-Hole Evaporation?, Phys. Rev. Lett. **46**, 1351 (1981).
[5] M. Visser, Hawking Radiation without Black Hole Entropy, Phys. Rev. Lett. **80**, 3436 (1998).
[6] M. Visser, Acoustic black holes: Horizons, ergospheres and Hawking radiation, Classical Quantum Gravity **15**, 1767 (1998).
[7] C. Barceló, S. Liberati, and M. Visser, Analogue gravity, Living Rev. Relativity **14**, 3 (2011).
[8] T. Jacobson, Black-hole evaporation and ultrashort distances, Phys. Rev. D **44**, 1731 (1991).
[9] W. G. Unruh, Sonic analogue of black holes and the effects of high frequencies on black hole evaporation, Phys. Rev. D **51**, 2827 (1995).
[10] S. Corley and T. Jacobson, Hawking spectrum and high frequency dispersion, Phys. Rev. D **54**, 1568 (1996).
[11] W. G. Unruh and R. Schützhold, Universality of the Hawking effect, Phys. Rev. D **71**, 024028 (2005).
[12] S. Corley and T. Jacobson, Black hole lasers, Phys. Rev. D **59**, 124011 (1999).
[13] S. Finazzi and R. Parentani, Black hole lasers in Bose–Einstein condensates, New J. Phys. **12**, 095015 (2010).
[14] L. J. Garay, J. R. Anglin, J. I. Cirac, and P. Zoller, Sonic Analog of Gravitational Black Holes in Bose-Einstein Condensates, Phys. Rev. Lett. **85**, 4643 (2000).
[15] P. O. Fedichev and U. R. Fischer, Gibbons-Hawking Effect in the Sonic de Sitter Space-Time of an Expanding Bose-Einstein-Condensed Gas, Phys. Rev. Lett. **91**, 240407 (2003).
[16] P. O. Fedichev and U. R. Fischer, Observer dependence for the phonon content of the sound field living on the effective curved space-time background of a Bose-Einstein condensate, Phys. Rev. D **69**, 064021 (2004).
[17] R. Schützhold, Detection Scheme for Acoustic Quantum Radiation in Bose-Einstein Condensates, Phys. Rev. Lett. **97**, 190405 (2006).
[18] I. Carusotto, S. Fagnocchi, A. Recati, R. Balbinot, and A. Fabbri, Numerical observation of Hawking radiation from acoustic black holes in atomic Bose–Einstein condensates, New J. Phys. **10**, 103001 (2008).
[19] A. Recati, N. Pavloff, and I. Carusotto, Bogoliubov theory of acoustic Hawking radiation in Bose-Einstein condensates, Phys. Rev. A **80**, 043603 (2009).
[20] J. Macher and R. Parentani, Black-hole radiation in Bose-Einstein condensates, Phys. Rev. A **80**, 043601 (2009).
[21] O. Lahav, A. Itah, A. Blumkin, C. Gordon, S. Rinott, A. Zayats, and J. Steinhauer, Realization of a Sonic Black Hole Analog in a Bose-Einstein Condensate, Phys. Rev. Lett. **105**, 240401 (2010).
[22] J. Steinhauer, Observation of quantum Hawking radiation and its entanglement in an analogue black hole, Nat. Phys. **12**, 959 (2016).
[23] C. Gooding, S. Biermann, S. Erne, J. Louko, W. G. Unruh, J. Schmiedmayer, and S. Weinfurtner, Interferometric Unruh Detectors for Bose-Einstein Condensates, Phys. Rev. Lett. **125**, 213603 (2020).
[24] U. Leonhardt, Cosmological horizons radiate, Europhys. Lett. **135**, 10002 (2021).
[25] J. R. Muñoz de Nova, K. Golubkov, V. I. Kolobov, and J. Steinhauer, Observation of thermal Hawking radiation and

its temperature in an analogue black hole, Nature (London) **569**, 688 (2019).
[26] V. I. Kolobov, K. Golubkov, J. R. Muñoz de Nova, and J. Steinhauer, Observation of stationary spontaneous Hawking radiation and the time evolution of an analogue black hole, Nat. Phys. **17**, 362 (2021).
[27] R. Balbinot, A. Fabbri, S. Fagnocchi, A. Recati, and I. Carusotto, Nonlocal density correlations as a signature of Hawking radiation from acoustic black holes, Phys. Rev. A **78**, 021603(R) (2008).
[28] J. Steinhauer, Measuring the entanglement of analogue Hawking radiation by the density-density correlation function, Phys. Rev. D **92**, 024043 (2015).
[29] U. Leonhardt, Questioning the recent observation of quantum Hawking radiation, Ann. Phys. (Berlin) **530**, 1700114 (2018).
[30] Y.-H. Wang, T. Jacobson, M. Edwards, and C. W. Clark, Induced density correlations in a sonic black hole condensate, SciPost Phys. **3**, 022 (2017).
[31] L. J. Garay, J. R. Anglin, J. I. Cirac, and P. Zoller, Sonic black holes in dilute Bose-Einstein condensates, Phys. Rev. A **63**, 023611 (2001).
[32] L. Santos, F. Floegel, T. Pfau, and M. Lewenstein, Continuous optical loading of a Bose-Einstein condensate, Phys. Rev. A **63**, 063408 (2001).
[33] A. P. Chikkatur, Y. Shin, A. E. Leanhardt, D. Kielpinski, E. Tsikata, T. L. Gustavson, D. E. Pritchard, and W. Ketterle, A continuous source of Bose-Einstein condensed atoms, Science **296**, 2193 (2002).
[34] M. Falkenau, V. V. Volchkov, J. Rührig, A. Griesmaier, and T. Pfau, Continuous Loading of a Conservative Potential Trap from an Atomic Beam, Phys. Rev. Lett. **106**, 163002 (2011).
[35] N. P. Robins, C. Figl, M. Jeppesen, G. R. Dennis, and J. D. Close, A pumped atom laser, Nat. Phys. **4**, 731 (2008).
[36] C.-C. Chen, S. Bennetts, R. G. Escudero, B. Pasquiou, and F. Schreck, Continuous Guided Strontium Beam with High Phase-Space Density, Phys. Rev. Applied **12**, 044014 (2019).
[37] P. C. Hohenberg, Existence of long-range order in one and two dimensions, Phys. Rev. **158**, 383 (1967).
[38] R. Schützhold, M. Uhlmann, Y. Xu, and U. R. Fischer, Quantum backreaction in dilute Bose-Einstein condensates, Phys. Rev. D **72**, 105005 (2005).
[39] U. Leonhardt, T. Kiss, and P. Öhberg, Theory of elementary excitations in unstable Bose-Einstein condensates and the instability of sonic horizons, Phys. Rev. A **67**, 033602 (2003).
[40] A. Coutant and R. Parentani, Black hole lasers, a mode analysis, Phys. Rev. D **81**, 084042 (2010).
[41] C. C. H. Ribeiro and D. A. T. Vanzella, Analogues of gravity-induced instabilities in anisotropic metamaterials, Phys. Rev. Research **2**, 013281 (2020).
[42] W. C. C. Lima and D. A. T. Vanzella, Gravity-Induced Vacuum Dominance, Phys. Rev. Lett. **104**, 161102 (2010).
[43] W. C. C. Lima, G. E. A. Matsas, and D. A. T. Vanzella, Awaking the Vacuum in Relativistic Stars, Phys. Rev. Lett. **105**, 151102 (2010).
[44] Y.-H. Wang, T. Jacobson, M. Edwards, and C. W. Clark, Mechanism of stimulated Hawking radiation in a laboratory Bose-Einstein condensate, Phys. Rev. A **96**, 023616 (2017).
[45] J. R. M. de Nova, D. Guéry-Odelin, F. Sols, and I. Zapata, Birth of a quasi-stationary black hole in an outcoupled Bose–Einstein condensate, New J. Phys. **16**, 123033 (2014).
[46] P.-E. Larré, A. Recati, I. Carusotto, and N. Pavloff, Quantum fluctuations around black hole horizons in Bose-Einstein condensates, Phys. Rev. A **85**, 013621 (2012).
[47] T. Paul, K. Richter, and P. Schlagheck, Nonlinear Resonant Transport of Bose-Einstein Condensates, Phys. Rev. Lett. **94**, 020404 (2005).
[48] J. Curtis, G. Refael, and V. Galitski, Evanescent modes and step-like acoustic black holes, Ann. Phys. (Amsterdam) **407**, 148 (2019).
[49] R. Seki, On boundary conditions for an infinite square-well potential in quantum mechanics, Am. J. Phys. **39**, 929 (1971).
[50] S. De Vincenzo and C. Sánchez, Point interactions: Boundary conditions or potentials with the Dirac delta function, Can. J. Phys. **88**, 809 (2010).
[51] P. Jain, A. S. Bradley, and C. W. Gardiner, Quantum de Laval nozzle: Stability and quantum dynamics of sonic horizons in a toroidally trapped Bose gas containing a superflow, Phys. Rev. A **76**, 023617 (2007).
[52] M. Tettamanti, S. L. Cacciatori, A. Parola, and I. Carusotto, Numerical study of a recent black-hole lasing experiment, Europhys. Lett. **114**, 60011 (2016).
[53] F. Michel and R. Parentani, Saturation of black hole lasers in Bose-Einstein condensates, Phys. Rev. D **88**, 125012 (2013).
[54] F. Michel and R. Parentani, Nonlinear effects in time-dependent transonic flows: An analysis of analog black hole stability, Phys. Rev. A **91**, 053603 (2015).
[55] J. R. M. de Nova, P. F. Palacios, I. Carusotto, and F. Sols, Long time universality of black-hole lasers, New J. Phys. **23**, 023040 (2021).
[56] L. P. Pitaevskii and S. Stringari, *Bose-Einstein Condensation*, International Series of Monographs on Physics (Clarendon Press, Oxford, 2003).
[57] I. Carusotto, S. X. Hu, L. A. Collins, and A. Smerzi, Bogoliubov-Cherenkov Radiation in a Bose-Einstein Condensate Flowing against an Obstacle, Phys. Rev. Lett. **97**, 260403 (2006).
[58] Y. Castin and R. Dum, Low-temperature Bose-Einstein condensates in time-dependent traps: Beyond the $U(1)$ symmetry-breaking approach, Phys. Rev. A **57**, 3008 (1998).
[59] R. Lopes, C. Eigen, N. Navon, D. Clément, R. P. Smith, and Z. Hadzibabic, Quantum Depletion of a Homogeneous Bose-Einstein Condensate, Phys. Rev. Lett. **119**, 190404 (2017).